



Defect studies of hydrogen-loaded nanocrystalline Gd films

J. Cizek^{a,*}, I. Prochazka^a, M. Vlach^a, N. Zaludova^a, S. Danis^a, G. Brauer^b, W. Anwand^b,
A. Mücklich^b, R. Gemma^c, R. Kirchheim^c, A. Pundt^c

^a Faculty of Mathematics and Physics, Charles University in Prague, V Holesovickach 2, CZ-180 00 Praha 8, Czech Republic

^b Institut für Ionenstrahlphysik und Materialforschung, Forschungszentrum Dresden-Rossendorf, Postfach 510119, D-01314 Dresden, Germany

^c Institut für Materialphysik, Universität Göttingen, Friedrich-Hund-Platz 1, D-37077 Göttingen, Germany

ARTICLE INFO

Article history:

Available online 15 May 2008

Keywords:

Nanocrystalline gadolinium films
Hydrogen
Slow positron implantation spectroscopy
X-ray diffraction

ABSTRACT

The present work reports on microstructure investigations of hydrogen-loaded nanocrystalline Gd films by means of slow positron implantation spectroscopy combined with *in situ* synchrotron radiation X-ray diffraction. It is found that the virgin films contain a high density of vacancy-like open volume defects at grain boundaries which trap positrons. These defects represent trapping sites also for hydrogen. With increasing hydrogen concentration the transformation from the α - into the β -phase (GdH_2) takes place in the film. Accumulation of hydrogen at grain boundaries causes a decrease of positron localization at defects. The transformation into the β -phase is completed at $x_{\text{H}} \approx 1.6$ H/Gd. Contrary to bulk Gd specimens, the γ -phase (GdH_3) is not formed in the nanocrystalline Gd films.

© 2008 Elsevier B.V. All rights reserved.

1. Introduction

The Gd–H system attracts attention of researchers because (i) it can absorb a large amount of hydrogen and exhibits a negative enthalpy of solution for atomic hydrogen [1], (ii) thin Gd films can be reversibly switched from optically refractive to transparent state by exposure to hydrogen [2]. The knowledge about the Gd–H phase diagram is yet incomplete, especially at low temperatures [1]. With increasing hydrogen concentration (expressed as atom ratio H/Gd throughout this paper) bulk Gd undergoes the following phase transition sequence: α -phase (hcp, GdH) \rightarrow β -phase (fcc, GdH_2) \rightarrow γ -phase (hcp, GdH_3). In the α -phase at room temperature, hydrogen solubility is very low ($x_{\text{H}} < 0.01$). Under normal conditions, Gd samples always contain some traces of the β -phase. With increasing hydrogen concentration, the volume fraction of the β -phase increases at the expense of the α -phase. At $x_{\text{H}} \approx 1.9$, the bulk sample is completely transformed into the β -phase. Formation of the γ -phase begins place from $x_{\text{H}} \approx 2.3$ and is completed at ≈ 2.8 .

Hydrogen-loaded thin films often behave very differently from the corresponding bulk materials [3]. It happens because of two main reasons: (i) contrary to free standing bulk samples which

exhibit isotropic lattice expansion when loaded with hydrogen, thin films are clamped to a substrate. The clamping prevents the in-plane lattice expansion and causes appearance of large in-plane compressive stresses (in the GPa range) [4], which influence the behavior of the loaded films. (ii) Thin films, and in particular nanocrystalline films, often exhibit a high density of lattice defects. It is known that H strongly interacts with defects [2]. Thus, the defect structure is an important factor which must be considered in investigations of hydrogen-loaded specimens.

Nanocrystalline Gd films loaded with hydrogen were studied in the present work. Defect studies of the films were performed by slow positron implantation spectroscopy (SPIS) utilizing monoenergetic slow-positron beam with adjustable energy. SPIS was combined with *in situ* X-ray diffraction (XRD) studies.

2. Experimental details

Thin Gd films were deposited on optically polished (11 $\bar{2}$ 0) sapphire substrates by cold cathode beam sputtering in an UHV chamber (10^{-10} mbar). As determined by transmission electron microscopy (TEM), film thickness was 1240 nm and films exhibited elongated column-like grains with a typical lateral width of ≈ 50 nm. The film surface was subsequently covered with a 30 nm thick Pd cap at room temperature in order to prevent oxidation, and to facilitate hydrogen absorption into the Gd layer [5]. The virgin films were firstly anodized at a constant potential of 0.8 V in order to remove hydrogen dissolved already in the as-deposited specimens. Subsequently, the films were step-by-step cathodically

* Corresponding author at: Department of Low-Temperature Physics, Faculty of Mathematics and Physics, Charles University, V Holesovickach 2, CZ-180 00 Praha 8, Czech Republic. Tel.: +420 2 21912788; fax: +420 2 2191 2567.

E-mail address: jakub.cizek@mff.cuni.cz (J. Cizek).

charged with hydrogen [6] in a galvanic cell filled with 1 M KOH electrolyte. The hydrogen concentration in the sample was calculated from the Faraday's Law. Bulk Gd (99.9%) samples, annealed at 700 °C for 1 h in vacuum (10^{-8} mbar), were used as reference samples for SPIS investigations.

The SPIS studies of thin films were performed at the magnetically guided positron beam facility "SPONSOR" [7] with a positron energy adjustable from 0.03 to 36 keV. Doppler broadening of the annihilation line was measured by an HPGe detector with an energy resolution of (1.09 ± 0.01) keV at 511 keV and characterized in terms of the S parameter. An energy window of 744 eV centered at 511 keV was used for evaluation of the S parameters. The *in situ* XRD investigations of hydrogen-loaded films were performed at HASYLAB (DESY, Hamburg) using synchrotron radiation with a wavelength $\lambda \approx 0.5$ Å.

3. Results and discussion

The dependence of the S parameter on positron energy E measured on the reference bulk Gd samples is plotted in Fig. 1A. Two bulk samples were compared: sample A was annealed at vacuum and its surface was subsequently covered with the Pd over-layer; sample B was also annealed at vacuum but its surface was not covered by Pd. For sample A, the S -values converge at high energies to a bulk value $S_0 = 0.5078(5)$. All the S parameters measured in this work were normalized to this value S_0 . It can be seen from Fig. 1A that S parameters measured at higher energies for the sample B reasonably converge the bulk value, too. From fitting of the $S(E)$ curves by VEPFIT [8] (solid lines in Fig. 1A) we obtained the bulk positron diffusion length $L_{+,Gd} = (270 \pm 30)$ and (280 ± 20) nm for the samples A and B, respectively. These diffusion lengths indicate that both reference Gd samples are well annealed and their bulk can be considered as a defect-free material. However, the structure of the subsurface region differs considerably in both reference samples. Sample A exhibits a drop of S at low energies due to positron annihilations inside the Pd cap. At higher energies, there is an increase of S caused by an increasing contribution of positron annihilations in Gd. The data indicate a broad maximum of S around 12 keV, which seems to be reflected also by VEPFIT results below. Subsequently, S decreases slightly to the bulk value. Thus, going from the surface into the depth, one can consider three regions in the sample A: (i) the Pd cap, (ii) a Gd subsurface layer, which exhibits slightly enhanced S parameter most probably due to damage caused by sputtering of the Pd cap, and (iii) a defect-free bulk Gd region. From fitting of the $S(E)$ curve it was found that the width of the layer (ii) is (120 ± 20) nm, and this layer exhibits a positron diffusion length of

(100 ± 10) nm. The Pd layer (i) is highly defected which is testified by a low positron diffusion length of (20 ± 5) nm, its width was fixed at 20 nm known from TEM. The $S(E)$ curve for the reference sample B exhibits a maximum at 7 keV due to positron annihilations inside the Gd oxide layer formed on the uncovered Gd surface exposed to air. Subsequently, S converges to the bulk value. Thus, the sample B consists of two layers only: (i) a Gd oxide layer and (ii) the bulk Gd region. The width of the oxide layer of (240 ± 20) nm was obtained from a fit of the $S(E)$ curve using this model. The positron diffusion length in the oxide layer is estimated to be (110 ± 10) nm.

The $S(E)$ curve for the virgin (unloaded) Gd film is plotted in Fig. 1B. The drop of S at low energies is due to positron annihilations inside the Pd cap. An increasing fraction of positrons annihilating inside the Gd layer causes an increase of S with increasing positron energy E . In the energy range from 5 to 11 keV almost all positrons annihilate inside the Gd layer, and S reaches a plateau-like value. Finally, at higher energies positrons begin to penetrate also into the sapphire substrate and this contribution causes a decrease of S . From comparison with the reference bulk samples it becomes clear that the Gd film exhibits a substantially higher S value. This is a consequence of nanoscale grain size, which leads to a significant volume fraction of grain boundaries and, thereby, a significant contribution of positrons trapped at open volume defects at grain boundaries. The trapped positrons raise the S parameter and decrease the positron diffusion length in the Gd layer. The $S(E)$ curves for Gd films were fitted by VEPFIT using a three-layer model: (i) Pd cap, (ii) Gd layer, and (iii) sapphire substrate. For the Pd cap we obtained practically the same results as those for Pd cap deposited on the reference sample A. The Gd layer exhibits the positron diffusion length of (168 ± 3) nm, i.e. shorter than that in defect-free Gd, due to positron trapping at grain boundaries. The sapphire substrate exhibits a rather short positron diffusion length of (38 ± 3) nm most probably due to positron trapping at dislocations introduced by polishing of the substrate surface.

The $S(E)$ curves measured on the films loaded to various hydrogen concentrations are plotted in Fig. 1B. Clearly, hydrogenation of the film causes a strong decrease of the S parameter for the Gd layer. The S parameters and positron diffusion lengths for the Gd layer obtained from fits of the $S(E)$ curves are plotted in Fig. 2A as a function of hydrogen concentration.

The XRD spectrum of the unloaded virgin film does not only contain reflections corresponding to the α -phase but also weak reflections which can be attributed to the β -phase. Thus, traces of the β -phase are present already in the unloaded virgin film. The out-of-plane lattice parameters of the α and the β -phase obtained

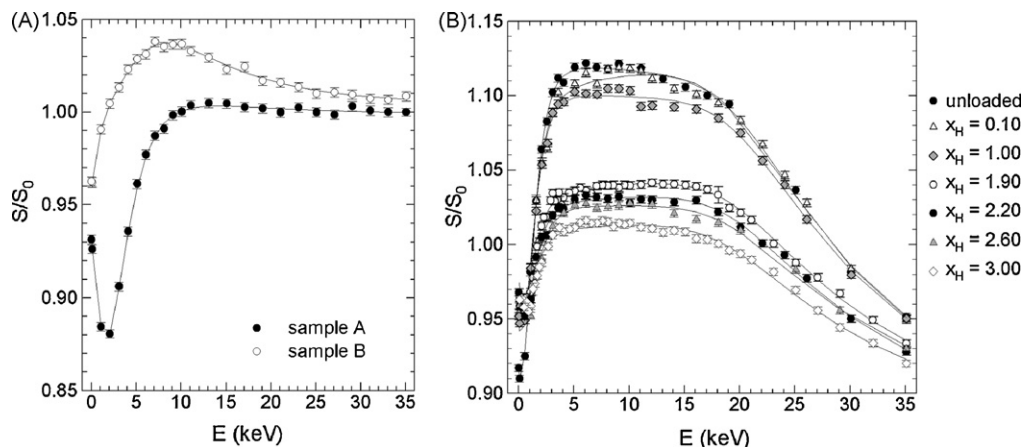


Fig. 1. The $S(E)$ curves for (A) the reference bulk Gd samples, (B) the Gd films loaded to various hydrogen concentrations. The solid lines show the fit of the curves by VEPFIT [8].

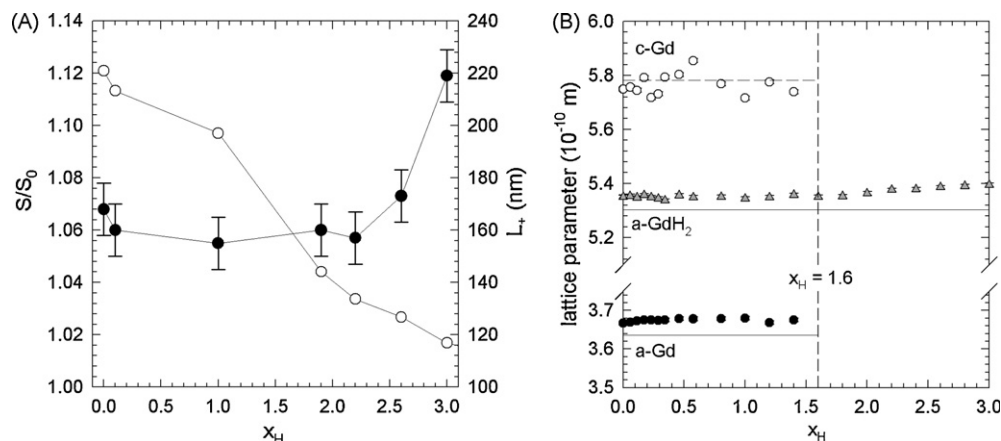


Fig. 2. (A) S parameter and the positron diffusion length L_+ for the Gd layer as obtained from fitting of the $S(E)$ curves by VEPFIT [8] and plotted as a function of hydrogen concentration, and (B) dependence of the lattice parameters of the α (hcp) and the β (fcc) phase on hydrogen concentration x_H . The lattice parameters were obtained from fitting of the XRD spectra. Solid lines show the lattice parameters for the bulk Gd.

from fitting of the XRD spectra are plotted in Fig. 2B as a function of hydrogen concentration. The lattice parameters known from the literature for bulk Gd [9] and GdH₂ [10] are shown in Fig. 2B by solid lines. The out-of-plane lattice parameter a measured in the film is higher than in bulk Gd. It testifies compressive in-plane stresses in the film. The c parameter is almost the same as that for bulk Gd. It is in concordance with texture measurements which revealed that the $(10\bar{1}0)$ fiber texture is the main texture component. With increasing hydrogen concentration, the α -phase transforms into the β -phase. It is seen as a gradual decrease of the intensity of the α -phase reflections while that of the β -phase reflections grows up. The lattice parameters of both phases remain approximately constant during the phase transition. At $x_H \approx 1.6$, the transformation is completed and the film contains only the β -phase. Thus, the two-phase field ($\alpha + \beta$) in the nanocrystalline Gd film is narrower compared to bulk Gd. Such narrowing was observed in a number of nanocrystalline metals [3]. A further increase of the hydrogen content causes only a broadening of the β -phase reflections and an expansion of the lattice seen as an increase of the lattice parameter a . Thus, one can conclude that the γ -phase is not formed in the nanocrystalline Gd film. Most probably for the nanocrystalline structure it is energetically more favorable to stay in the β -phase. The increase of the hydrogen concentration makes the film structure less defined (i.e. local variations of the lattice constant become larger) which is seen by a broadening of the diffraction profiles.

From the comparison of SPIS and XRD results we can conclude that the strong decrease of the S parameter for the Gd layer observed in the hydrogenated film occurs mainly due to transition from the α -phase into the β -phase. In addition, hydrogen fills the open volume defects and grain boundaries which exhibit a more open structure. It lowers the ability of defects to trap positrons and increases the local electron density at defects. Both effects

contribute to a lowering of S and an increase of the positron diffusion length in the Gd layer.

4. Conclusions

Nanocrystalline Gd films with thickness of 1240 nm were deposited on sapphire substrate and step-by-step loaded with hydrogen. SPIS studies show a strong decrease of the S parameter for the Gd layer caused by α to β phase transition and hydrogenation of grain boundaries. Traces of the β phase are found to be present already in the virgin film. The two-phase field ($\alpha + \beta$) is found to be narrower compared to bulk Gd. The γ -phase is found to not form at high hydrogen concentrations.

Acknowledgements

Financial support from The Czech Science Foundation (project No. 202/05/0074), The Ministry of Education, Youth and Sports of The Czech Republic (project No. MS 0021620834) and The Alexander von Humboldt Foundation is highly acknowledged.

References

- [1] F.B. Manchester (Ed.), Phase Diagrams of Binary Hydrogen Alloys., ASM International, Materials Park, 2000, p. 58.
- [2] J.N. Huijberts, R. Griessen, J.H. Rector, R.J. Wijngaarden, J.P. Dekker, D.G. de Groot, N.J. Koeman, Nature 380 (1996) 231.
- [3] A. Pundt, R. Kirchheim, Annu. Rev. Mater. Res. 36 (2006) 55.
- [4] U. Laudahn, A. Pundt, M. Bicker, U.V. Hülsen, U. Geyer, T. Wagner, R. Kirchheim, J. Alloys Compd. 293–295 (1999) 490.
- [5] M.A. Pick, J.W. Davenport, M. Strongin, G.J. Dienes, Phys. Rev. Lett. 43 (1979) 286.
- [6] R. Kirchheim, Prog. Mat. Sci. 32 (1988) 261.
- [7] W. Anwand, H.-R. Kissener, G. Brauer, Acta Phys. Polonica A 88 (1995) 7.
- [8] A. van Veen, H. Schut, M. Clement, J. de Nijs, A. Kruseman, M. Ijpm, Appl. Surf. Sci. 85 (1995) 216.
- [9] F.J. Darnell, Phys. Rev. 130 (1963) 1825.
- [10] M. Ellner, H. Reule, E.J. Mittemeijer, J. Alloys Compd. 279 (1998) 179.